frontiers | Frontiers in Nutrition

TYPE Original Research
PUBLISHED 28 July 2025
DOI 10.3389/fnut.2025.1639554

OPEN ACCESS

EDITED BY
Jinyan Gong,
Zhejiang University of Science and Technology, China

REVIEWED BY
Yongsheng Chen,
Jinan University, China
Qun Wang,
South China Agricultural University, China

*CORRESPONDENCE
Wupeng Ge
✉ josephge@nwafu.edu.cn

RECEIVED 02 June 2025
ACCEPTED 01 July 2025
PUBLISHED 28 July 2025

CITATION
Gao P, Nie Y, Zhou Y and Ge W (2025) Preparation, characterization, and application of camellianin A/soy protein isolate covalent complexes.
Front. Nutr. 12:1639554.
doi: 10.3389/fnut.2025.1639554

Preparation, characterization, and application of camellianin A/soy protein isolate covalent complexes

Peng Gao[1], Yuanyang Nie[2], Yingxuan Zhou[2] and Wupeng Ge[1]*

[1]College of Food Science and Engineering, Northwest A&F University, Yangling, China, [2]School of Food Science, Henan Institute of Science and Technology, Xinxiang, China

Alkaline-assisted processing facilitated the development of camellianin A (CA)-soy protein isolate (SPI) conjugates, with systematic characterization of polyphenol incorporation effects on macromolecular architecture and emulsion stabilization capacity. Multi-spectroscopic profiling confirmed CA-induced structural reorganization of SPI matrices, verifying conjugate formation. Dose-dependent enhancement patterns were observed, where increased CA loading positively correlated with total phenolic content, surface hydrophilicity, ABTS radical scavenging activity and reducing power. The derived nanoemulsions demonstrated superior oxidative stabilization capacity and storage stability, outperforming SPI-only stabilized systems. Our results can advance the utilization of CA in functional foods, providing practical guidance for developing novel food-grade nanoemulsions with enhanced delivery efficacy.

KEYWORDS

camellianin A, soy protein isolate, covalent complex, nanoemulsion, characterization

1 Introduction

Interactions between proteins and polyphenols are inevitable in food matrices, leading to modifications in their structural configurations, functional properties, and physicochemical characteristics, which subsequently influence food flavor, color, and nutritional value (1, 2). These interactions primarily occur through two distinct mechanisms: covalent and non-covalent binding. Non-covalent associations, mediated by electrostatic forces, hydrophobic interactions, hydrogen bonding, electrostatic forces, and van der Waals attractions, are generally reversible and susceptible to environmental changes (3). In contrast, covalent conjugation between polyphenols and proteins forms stable polymeric complexes that can significantly enhance protein functionality, including improved emulsifying capacity, increased antioxidant activity, and reduced allergenicity under specific conditions (4, 5). Notably, Liu et al. (6) demonstrated that radical-induced coupling of β-lactoglobulin with chlorogenic acid enhanced both thermal stability and antioxidant properties of the protein. Covalent conjugation has been widely employed in functional food development for encapsulating and controlling the release of bioactive compounds, thereby improving their bioavailability and stability (7, 8). For instance, Gu et al. (9) prepared ovalbumin-catechin conjugates via free radical grafting, revealing that polyphenol incorporation not only augmented the protein's antioxidant capacity but also effectively suppressed β-carotene oxidation while enhancing its biological utilization.

Soy protein isolate (SPI), containing all essential amino acids, is widely utilized in food industry due to its excellent functional properties including superior emulsifying capacity and gelation ability (10). However, its susceptibility to denaturation under extreme pH, high ionic

strength, or elevated temperatures often compromises its functionality, thereby limiting applications in complex food systems (11). Camellianin A (CA), the predominant flavonoid (>20% content) in *Adinandra nitida* leaves, possesses remarkable bioactivities (12). Liu et al. (13) demonstrated its potent antioxidant capacity, while Gao et al. (14) reported significant inhibitory effects on HepG2 and MCF-7 cancer cell proliferation. Jia et al. (15) further identified its α-glucosidase inhibitory activity. Although Zhou et al. (16) investigated non-covalent CA-lysozyme complexes for nanoemulsion stabilization, covalent conjugation between CA and food-grade proteins remains unexplored. This study pioneers the covalent conjugation of CA with SPI, systematically characterizing the structural modifications and functional enhancements of the resultant complexes. The research specifically evaluates their application in nanoemulsions as novel emulsifiers.

2 Materials and methods

2.1 Chemicals

CA was from our previous report (16). Soy protein isolate (SPI) was provided by Mantianxue Food Manufacturing Co., Ltd. (Anyang, China). The sunflower oil was the product of COFCO Fulinmen Food Marketing Co., Ltd. (Beijing, China). Medium-chain triglycerides (MCT), 8-Anilino-1-naphthalenesulfonic acid (ANS), 2,2′-Azino-bis(3-ethylbenzothiazoline-6-sulfonic acid) diammonium salt (ABTS), and Folin–Ciocalteu's phenol reagent were purchased from Yuanye Biological Technology Co., Ltd. (Shanghai, China). All other reagents were of analytical grade.

2.2 Preparation of CA/SPI covalent complex

The CA/SPI covalent complexes were prepared through an alkaline-induced method (17). Specifically, SPI was dissolved in 100 mL deionized water and adjusted to pH 9.0 using 0.5 mol/L NaOH solution to obtain a 0.5 wt% protein solution. The solution was allowed to swell overnight at 4°C to ensure complete hydration, with sodium azide (0.005%) added as a microbial inhibitor. For covalent conjugation, 100 mL of CA solution at varying concentrations (0.02 wt%, 0.05 wt%, and 0.1 wt%) was gradually added to 100 mL of the protein solution under constant stirring. The reaction mixture was readjusted to pH 9.0 with 0.5 mol/L NaOH and maintained for 24 h. Subsequently, the resulting complexes were dialyzed (molecular weight cutoff: 3,500 Da) for 48 h and lyophilized to obtain the final products, designated as CA/SPI-1, CA/SPI-2, and CA/SPI-3 corresponding to the increasing CA concentrations.

2.3 UV and FT-IR spectra

The UV spectra (220–400 nm) of CA, SPI, and CA/SPI covalent complexes were acquired using a TU-1810 spectrophotometer (Persee Analytical, China). Fourier-transform infrared (FT-IR) spectra (4000 to 400 cm^{-1}) was collected on a Bruker INVENIO spectrometer (Bruker Optics, Germany).

2.4 Determination of total phenolic content

The total phenolic contents (TPC) of the three CA/SPI covalent complexes were analyzed based on the Folin–Ciocalteu method (18). Sample solutions were prepared at a concentration of 5 mg/mL. For analysis, 0.3 mL of each sample solution was diluted to 10 mL with distilled water, followed by addition of 0.5 mL Folin–Ciocalteu reagent. After vortexing for 5 min, 5 mL of Na_2CO_3 (5% w/v) was added, and the final volume was adjusted to 25 mL with H_2O. The reaction mixtures were incubated in the dark for 90 min before measuring absorbance at 750 nm against an ultrapure water blank. TPC was calculated based on a standard curve prepared with CA and expressed as mg CA equivalents per g sample (mg CAE/g).

2.5 Fluorescence spectra

Sample solutions of SPI, CA/SPI-1, CA/SPI-2, and CA/SPI-3 were prepared at a concentration of 1 mg/mL using 10 mmol/L PBS buffer (pH 7.0). Fluorescence emission spectra (300–450 nm) at $\lambda_{ex} = 280$ was collected on a fluorescence spectrophotometer.

2.6 Surface hydrophobicity measurement

The surface hydrophobicity values of SPI, CA/SPI-1, CA/SPI-2, and CA/SPI-3 were evaluated using ANS as a fluorescent probe (19). SPI and three CA/SPI covalent complexes were diluted to concentrations of 0.05–0.30 mg/mL with 10 mmol/L PBS (pH 6.5). For each measurement, 20 μL of ANS solution (8×10^{-3} mol/L) was added to 4 mL of protein solution and mixed thoroughly. After 10 min of incubation in the dark, fluorescence emission spectra (400–700 nm) were recorded at $\lambda_{ex} = 390$ nm using a fluorescence spectrophotometer. The maximum fluorescence intensity was plotted against protein concentration, with the slope of the resulting linear regression representing the relative surface hydrophobicity index (H_0).

2.7 Determination of ABTS radical scavenging activity

The ABTS radical scavenging assay of CA, SPI, and CA/SPI covalent complexes was carried out based on the report of Gu et al. (20). The ABTS test solution was prepared by mixing 200 mL of 7 mmol/L ABTS stock solution with 3.52 mL of 2.45 mmol/L potassium persulfate solution, followed by 12 h incubation in the dark at room temperature. The resulting solution was diluted with 0.05 mol/L PBS (pH 7.4) to achieve an absorbance of 0.70 ± 0.02 at 734 nm after 30 min equilibration. For the assay, 0.15 mL of sample solution at various concentrations was mixed with 2.85 mL of the diluted ABTS radical test solution. After vortexing and 10 min reaction in the dark at room temperature, the absorbance (A_t) was measured at 734 nm using a spectrophotometer. A control measurement (A_0) was performed using 0.15 mL deionized water

instead of sample solution. The ABTS radical scavenging activity was calculated as Equation 1:

$$\text{ABTS scavenging activity}(\%) = \left[1 - \left(A_t / A_0\right)\right] \times 100 \quad (1)$$

2.8 Reducing power assay

The reducing power of CA, SPI, and CA/SPI covalent complexes was evaluated following the method established by Du et al. (21). In brief, 0.5 mL of sample solution at various concentrations was mixed with 2.5 mL of 0.2 mol/L PBS (pH 6.6) and 2.5 mL of 1% potassium ferricyanide solution. The mixture was vortexed thoroughly and incubated at 50°C for 20 min. After rapid cooling in an ice-water bath, 2.5 mL of 10% trichloroacetic acid solution was added, followed by centrifugation at 4,500 rpm for 10 min. Subsequently, 2.5 mL of the supernatant was combined with 2.5 mL ultrapure water and 0.5 mL of 0.1% ferric chloride solution. The reaction mixture was kept at room temperature for 10 min before measuring the absorbance at 700 nm using a spectrophotometer. The reducing power was expressed as the absorbance at 700 nm.

2.9 Preparation of nanoemulsions of CA/SPI covalent complexes

The nanoemulsions were prepared based on a previous report (22). Briefly, SPI and three CA/SPI covalent complexes (CA/SPI-1, CA/SPI-2, CA/SPI-3) were individually dissolved in ultrapure water at 4% (w/v) concentration to form the aqueous phase, while MCT served as the oil phase. The two phases were mixed at a 95:5 (v/v) ratio and homogenized at 15,000 rpm for 2 min to obtain coarse emulsions. For nanoemulsification, aliquots of the coarse emulsion were subjected to ultrasonic treatment using a probe sonicator under the following optimized parameters: 5 min total processing time at 660 W power output, with 2 s pulse-on and 2 s pulse-off intervals. The temperature was maintained below 25°C throughout sonication by employing an ice-water bath.

2.10 Storage stability evaluation of nanoemulsions

The storage stability of nanoemulsions prepared with SPI, CA/SPI-1, CA/SPI-2, and CA/SPI-3 was systematically evaluated under two temperature conditions (4°C and 25°C). At predetermined intervals, the emulsions were characterized for droplet size distribution using a Nano-ZS dynamic light scattering analyzer (Malvern Instruments, United Kingdom) (23). Prior to analysis, samples were diluted 1,000-fold with ultrapure water to minimize multiple scattering effects.

2.11 Evaluation of lipid oxidation resistance

Nanoemulsions containing SPI, CA/SPI-1, CA/SPI-2, and CA/SPI-3 were prepared according to Section 2.9, using sunflower oil as the oil phase. The emulsions were stored at 37°C to accelerate oxidation, with periodic determination of peroxide values (PV) (24). Briefly, 200 μL of emulsion was mixed with 1.5 mL of isooctane/2-propanol (3:1, v/v) in a 10 mL centrifuge tube through three cycles of 10 s vortex mixing. After centrifugation at 2,000 × g for 5 min and 3 min standing, 200 μL of the upper organic phase was transferred to a test tube containing 2.8 mL of methanol/1-butanol (2:1, v/v), followed by sequential addition of 15 μL ammonium thiocyanate solution (3.94 M) and 15 μL ferrous ion solution. The mixture was vortexed and incubated at room temperature for 20 min before measuring absorbance at 510 nm against a blank consisting of pure sunflower oil. Hydrogen peroxide concentration was determined from a standard calibration curve.

2.12 Statistical analysis

Experimental results are presented as mean value ± standard deviation ($n = 3$). Statistical analysis were performed using SPSS 26.0 (IBM Corp., United States), including ANOVA, Pearson correlation analysis, and Duncan's multiple comparison (significance level set at $p < 0.05$). Data visualization was conducted using Origin 8.0 (OriginLab Corp., United States).

3 Results and discussion

3.1 UV analysis

UV spectroscopy is widely employed to investigate interactions between proteins and polyphenols. This technique is particularly valuable because aromatic amino acid residues (e.g., tyrosine, phenylalanine, tryptophan) and sulfur-containing amino acids in proteins exhibit characteristic UV absorption (25). Changes in absorption peak positions and intensity can indicate molecular interactions between proteins and polyphenols. As shown in Figure 1, increasing the concentration of CA during preparation led to significant alterations in both the intensity and position of UV

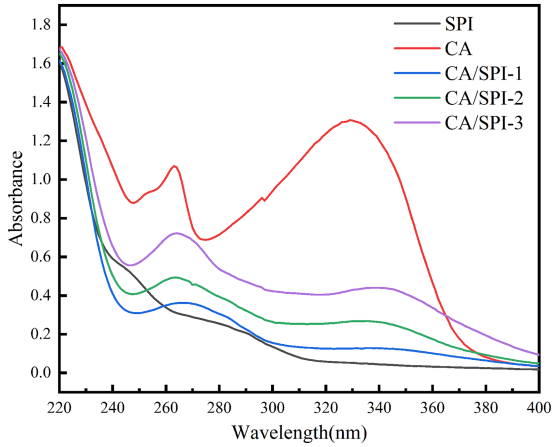

FIGURE 1
UV spectra of CA, SPI and their covalent complexes.

absorption peaks. Compared to pure SPI, the covalent complexes exhibited a blue shift of 2–10 nm in their absorption maxima. This spectral shift provides direct evidence of intermolecular interactions between CA and SPI, resulting in the formation of new chemical structures with modified electronic transitions.

3.2 FT-IR analysis

FT-IR can characterize the structural modifications in CA, SPI, and their covalent complexes (Figure 2). The spectrum of CA displayed characteristic absorption bands at 3393.92 cm^{-1} (O–H stretching), 2,920 cm^{-1} (C–H stretching), and 1630.38 cm^{-1} (C=O stretching). For SPI, the absorption peaks appeared at 3405.32 cm^{-1} (O–H/N–H stretching), 2961.01 cm^{-1} (C–H stretching), 1660.89 cm^{-1} (C=O stretching), and 1534.68 cm^{-1} (C–N stretching/N–H bending). The covalent complexes (CA/SPI-1, CA/SPI-2, and CA/SPI-3) exhibited absorption bands at 3400.76–3409.87 cm^{-1}, showing slight shifts from the original O–H/N–H vibrations of SPI and CA, suggesting potential hydrogen bond formation or covalent linkage through hydroxyl/amino groups. The persistent peaks at 2961.01–2965.6 cm^{-1} confirmed the preservation of aliphatic structures in the complexes. The amide I band shifted to 1650.89 cm^{-1}, indicating alterations in the C=O vibrational environment, while the amide II bands at 1534.68–1539.24 cm^{-1} demonstrated modified N–H/C–N vibrations. The overall spectral patterns predominantly reflected SPI's characteristic peaks, confirming its structural dominance in the complexes.

3.3 Total phenolic content

In this study, the Folin–Ciocalteu method was applied to quantify the content of CA covalently conjugated with SPI. The alkali-induced synthesis yielded CA/SPI covalent complexes with polyphenol contents of 126.65 ± 2.17 mg/g, 148.72 ± 2.84 mg/g, and 165.59 ± 6.66 mg/g, respectively. The results indicated a positive correlation between the incorporated total phenolic content and the increasing CA addition levels. Structural analysis revealed that the phenolic hydroxyl groups in CA could effectively graft onto nucleophilic groups (e.g., amino and sulfhydryl groups) of SPI through the oxidized quinone pathway, ultimately forming CA/SPI covalent complexes.

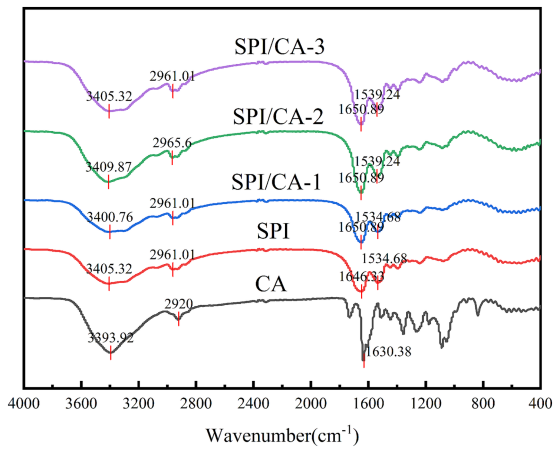

FIGURE 2
FT-IR spectra of CA, SPI and their covalent complexes.

3.4 Fluorescence analysis

The aromatic amino acids in proteins, including tryptophan (Trp), tyrosine (Tyr), and phenylalanine (Phe), exhibit intrinsic fluorescence under specific excitation wavelengths due to their conjugated double-bond systems (26). These residues emit light at longer wavelengths than the incident radiation within nanoseconds. Alterations in the microenvironment of these fluorophores can be monitored through fluorescence spectral changes, thereby enabling structural characterization of protein-polyphenol interactions (27). In Figure 3, SPI displayed a characteristic fluorescence emission peak near 340 nm, consistent with typical protein fluorescence profiles. Notably, the CA/SPI complex demonstrated significant fluorescence intensity reduction compared to native SPI, indicating polyphenol-induced fluorescence quenching. This phenomenon may arise from structural proximity between CA and SPI's fluorophores (e.g., Trp residues), where molecular interactions modulate excited-state energy dissipation.

3.5 Surface hydrophobicity analysis

The surface hydrophobicity of proteins serves as a critical indicator for monitoring structural modifications (28). In this study, ANS was selected as the fluorescent probe to detect alterations in nanoparticle surface hydrophobicity. Surface hydrophobicity reflects the distribution pattern of hydrophobic amino acid residues on protein surfaces, where higher values correspond to greater exposure of these hydrophobic moieties (29). In Figure 4, SPI exhibited progressively diminished surface hydrophobicity with increasing CA concentrations. The fluorescence attenuation percentages followed this descending order: CA/SPI-3 (53.28%) > CA/SPI-2 (42.76%) > CA/SPI-1 (8.58%). This phenomenon may be associated with (a) molecular interactions between CA and hydrophobic domains of SPI, and/or (b) structural reorganization of the protein that modulates the spatial distribution of hydrophobic regions in aqueous systems.

3.6 ABTS radical scavenging activity

The ABTS test represents a widely adopted method for evaluating antioxidant capacity. Oxidized ABTS forms a stable bluish-green cationic radical (ABTS) exhibiting maximum absorbance at 734 nm (30). The scavenging rate against ABTS radicals quantitatively reflects antioxidant potency, with higher values indicating superior activity. As presented in Table 1 and Figure 5, CA, SPI, and their complexes demonstrated concentration-dependent radical scavenging capacities positively correlated with total phenolic content. The calculated IC_{50} values of CA/SPI complexes were significantly lower than those of SPI alone, with antioxidant enhancements reaching 29.14, 48.96, and 67.54%, respectively. These findings suggest structural integration between CA and SPI synergistically amplifies antioxidant

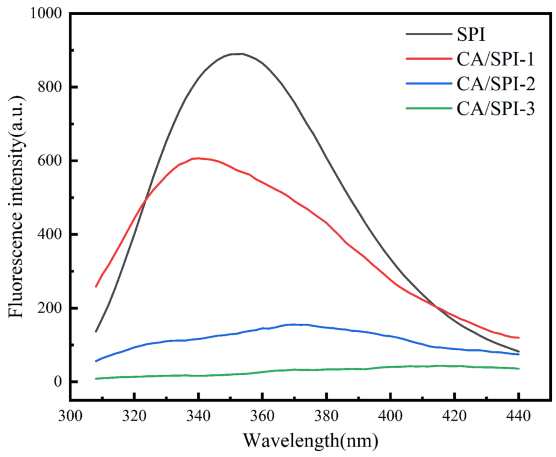

FIGURE 3
Fluorescence spectra of SPI and CA/SPI covalent complexes.

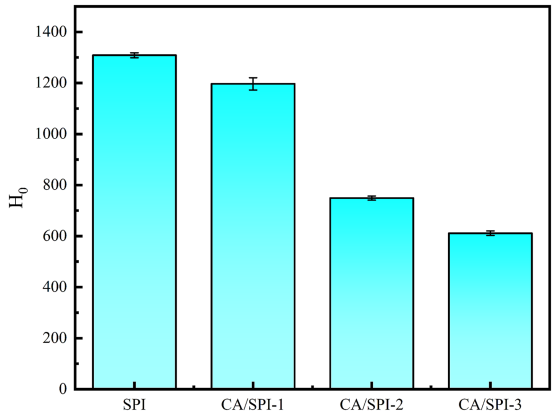

FIGURE 4
Surface hydrophobicity analysis of SPI and CA/SPI covalent complexes.

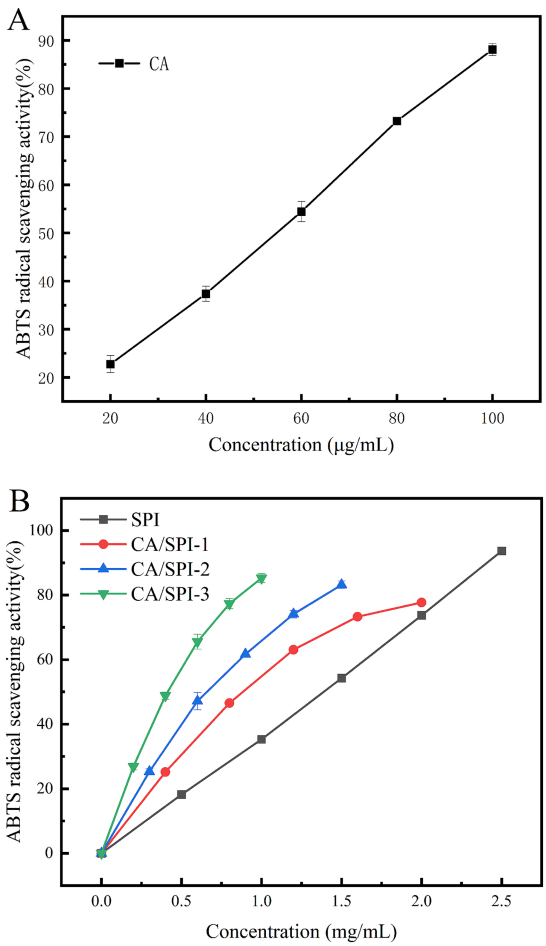

FIGURE 5
ABTS radical scavenging abilities of CA **(A)**, SPI and their CA/SPI **(B)** covalent complexes.

TABLE 1 ABTS radical scavenging abilities of CA, SPI and CA/SPI covalent complexes.

Sample	IC_{50} (μg/mL)
CA	46.50 ± 0.46[e]
SPI	1193.29 ± 4.94[a]
CA/SPI-1	845.61 ± 5.95[b]
CA/SPI-2	609.05 ± 8.02[c]
CA/SPI-3	387.37 ± 1.13[d]

[a-e] Subsequently, the resulting complexes were dialyzed (molecular weight cutoff: 3,500 Da) for 48 h and lyophilized to obtain the final products, designated as CA/SPI-1, CA/SPI-2, and CA/SPI-3 corresponding to the increasing CA concentrations.

performance. Such enhancement may be associated with redox-active moieties in the composite system, particularly hydroxyl-containing structures known to facilitate electron transfer processes (31).

3.7 Reducing power analysis

The iron-reducing capacity reflects a substance's ability to reduce Fe^{3+} to Fe^{2+}, serving as a critical indicator of antioxidant potential. Protein-polyphenol complexes can mediate the reduction of potassium ferricyanide [$K_3Fe(CN)_5$] to ferrous ions, subsequently reacting with $FeCl_3$ to form Prussian blue ($Fe_4[Fe(CN)_6]_3$), which exhibits a characteristic absorption peak at 700 nm. The absorbance intensity positively correlates with reducing capacity (32). As illustrated in Figure 6, CA demonstrated the highest reducing capacity, followed by CA/SPI complexes. At 10.0 mg/mL concentration, the CA/SPI-1, CA/SPI-2, and CA/SPI-3 complexes exhibited 1.21-, 1.32-, and 1.86-fold higher reducing capacities than native SPI, respectively, showing positive correlation with total phenolic content. These findings align with the report of Yi et al. (33) on catechin-α-lactalbumin systems, where phenolic conjugation significantly enhanced reducing performance. Collectively, the data suggest that polyphenol-mediated protein modification effectively amplifies iron-reducing capabilities in composite systems.

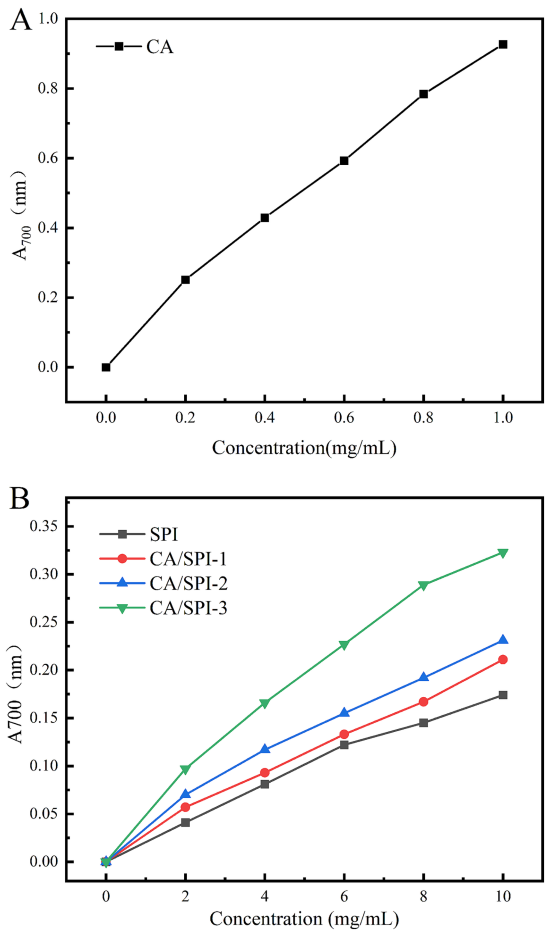

FIGURE 6
Reducing power analysis of CA **(A)**, SPI and their CA/SPI **(B)** covalent complexes.

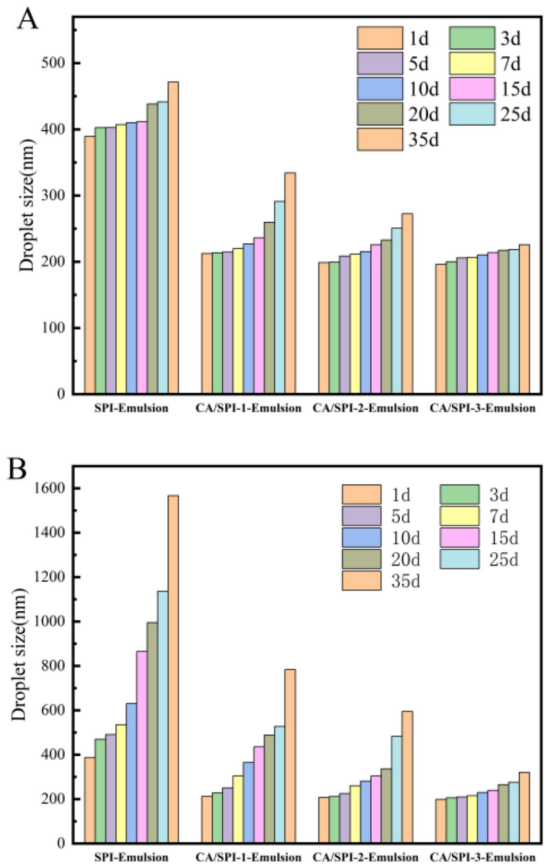

FIGURE 7
Changes in particle size of the nanoemulsions during storage at 4°C **(A)** and 25°C **(B)**.

3.8 Storage stability analysis

Physical stability during processing, transportation, and storage constitutes a critical parameter for emulsion applications. Temperature variations critically influence emulsion destabilization patterns, with droplet size serving as a key indicator of droplet aggregation status (34). Smaller initial droplet diameters (<300 nm) typically correlate with enhanced stability against phase separation. Systematic monitoring of four emulsion systems during 35-day storage at 4°C and 25°C revealed distinct stabilization profiles (Figure 7). Freshly prepared SPI-Emulsion exhibited an initial particle size of ~390 nm, while CA/SPI-derived nanoemulsions maintained diameters around 210 nm. Storage-induced particle growth proved most pronounced in SPI-Emulsion, culminating in phase separation at 25°C after 35 days. In contrast, CA/SPI-3-Emulsion retained sub-330 nm diameters under both storage conditions, with significantly attenuated growth rates at 4°C versus 25°C. The observed thermal activation effects on particle aggregation suggest temperature-modulated molecular mobility influences destabilization kinetics. Improved stabilization in CA/SPI systems likely stems from reinforced interfacial architecture capable of counteracting thermodynamic destabilization drivers.

3.9 Anti-lipid oxidation analysis

The enhanced surface-area-to-volume ratio of nanoemulsions facilitates interfacial interactions between lipid components and pro-oxidants, potentially accelerating oxidation kinetics (35, 36). Sunflower oil-based systems, characterized by elevated unsaturated fatty acid content (predominantly oleic and linoleic acids), demonstrated progressive lipid oxidation during 15-day storage at 37°C. Peroxide value evolution, as shown in Figure 8, revealed oxidation inhibition capacities in the descending order: CA/SPI-3 > CA/SPI-2 > CA/SPI-1 > SPI, correlating with phenolic constituent levels. Santos et al. (37) also found that the lipid oxidation inhibitory capacities gradually increased with the increase of polyphenol content when constructing the sodium caseinate/quercetin emulsion system.

4 Conclusion

Alkaline-assisted processing enables the formation of CA/SPI conjugates, as evidenced by structural modifications detected

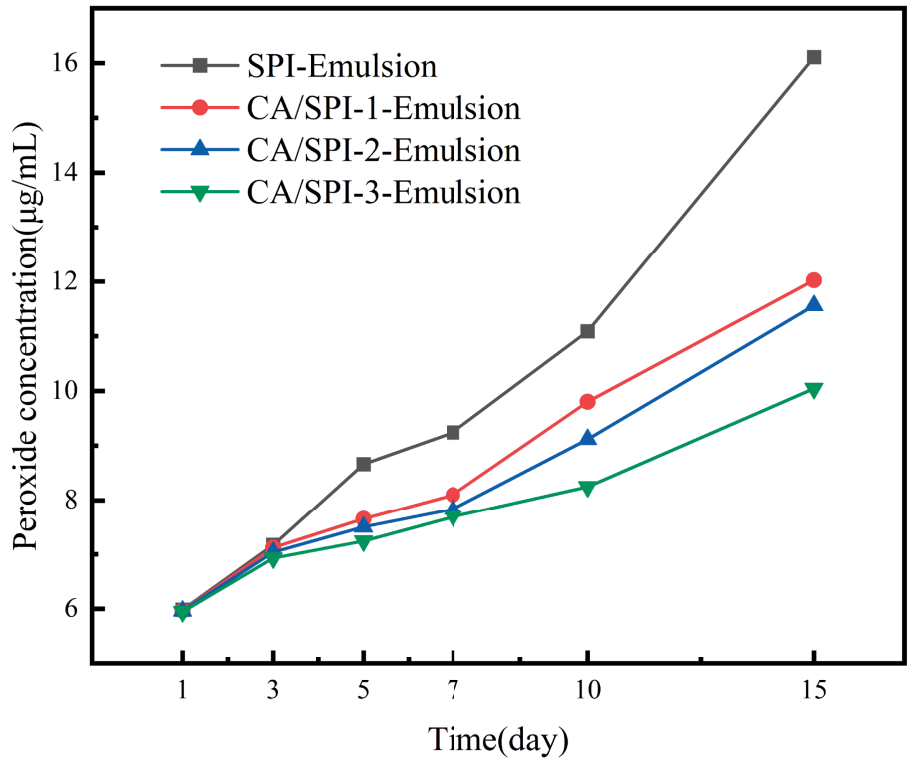

FIGURE 8
Peroxide content changes in nanoemulsions during storage.

through UV, FT-IR, and FS. The conjugated systems exhibited enhanced antioxidant capacity and hydrophilicity compared to native SPI, with the derived nanoemulsions demonstrating superior oxidative stability and storage performance. When employed as emulsifiers, CA/SPI conjugates generated nanoemulsions with droplet diameters below 220 nm, surpassing SPI-stabilized systems in lipid oxidation resistance during extended storage. These findings highlight the potential of polyphenol-modified protein complexes as functional emulsifiers for bioactive delivery applications in nutraceutical formulations.

Data availability statement

The raw data supporting the conclusions of this article will be made available by the authors, without undue reservation.

Author contributions

PG: Data curation, Formal analysis, Investigation, Writing – original draft, Writing – review & editing. YN: Data curation, Formal analysis, Investigation, Writing – original draft. YZ: Data curation, Formal analysis, Validation, Writing – original draft. WG: Funding acquisition, Project administration, Resources, Supervision, Visualization, Writing – original draft, Writing – review & editing.

Funding

The author(s) declare that financial support was received for the research and/or publication of this article. This research was funded by Shaanxi Province Key Research and Development Project (2021ZDLNY02-09), Xianyang City Key Research and Development Project (2021ZDYF-NY-0005), and School-Enterprise Cooperation Project (K4050423284).

Acknowledgments

The authors thank the participants and professionals involved in this study.

Conflict of interest

The authors declare that the research was conducted in the absence of any commercial or financial relationships that could be construed as a potential conflict of interest.

Generative AI statement

The authors declare that no Gen AI was used in the creation of this manuscript.

Publisher's note

References

1. Quan TH, Benjakul S, Sae-leaw T, Balange AK, Maqsood S. Protein–polyphenol conjugates: antioxidant property, functionalities and their applications. *Trends Food Sci Technol*. (2019) 91:507–17. doi: 10.1016/j.tifs.2019.07.049

2. Tazeddinova D, Rahman MR, Bin Hamdan S, Matin MM, Bin Bakri MK, Rahman MM. Plant based polyphenol associations with protein: a prospective review. *Bioresources*. (2022) 17:7110–34. doi: 10.15376/biores.17.4.tazeddinova2

3. Le Bourvellec C, Renard CMGC. Interactions between polyphenols and macromolecules: quantification methods and mechanisms. *Crit Rev Food Sci Nutr*. (2012) 52:213–48. doi: 10.1080/10408398.2010.499808

4. Xu Y, Wei Z, Xue C, Huang Q. Covalent modification of zein with polyphenols: a feasible strategy to improve antioxidant activity and solubility. *J Food Sci*. (2022) 87:2965–79. doi: 10.1111/1750-3841.16203

5. Xu PW, Yue XJ, Yuan XF, Zhao B. Covalent modification using hemp seed polyphenols improves the structural and functional properties of the hemp seed globulin. *Food Biosci*. (2023) 56:103293. doi: 10.1016/j.fbio.2023.103293

6. Liu J, Song G, Zhou L, Yuan Y, Wang D, Yuan T, et al. Sonochemical effects on fabrication, characterization and antioxidant activities of β-lactoglobulin-chlorogenic acid conjugates. *Ultrason Sonochem*. (2023) 92:106240. doi: 10.1016/j.ultsonch.2022.106240

7. Zhang K, Huang J, Wang D, Wan X, Wang Y. Covalent polyphenols-proteins interactions in food processing: formation mechanisms, quantification methods, bioactive effects, and applications. *Front Nutr*. (2024) 11:1371401. doi: 10.3389/fnut.2024.1371401

8. Baba WN, McClements DJ, Maqsood S. Whey protein–polyphenol conjugates and complexes: production, characterization, and applications. *Food Chem*. (2021) 365:130455. doi: 10.1016/j.foodchem.2021.130455

9. Gu L, Su Y, Zhang M, Chang C, Li J, McClements DJ, et al. Protection of β-carotene from chemical degradation in emulsion-based delivery systems using antioxidant interfacial complexes: catechin-egg white protein conjugates. *Food Res Int*. (2017) 96:84–93. doi: 10.1016/j.foodres.2017.03.015

10. Liu F, Tang CH. Soy protein nanoparticle aggregates as Pickering stabilizers for oil-in-water emulsions. *J Agric Food Chem*. (2013) 61:8888–98. doi: 10.1021/jf401859y

11. Shan H, Lu S, Jiang L, Wang L, Liao H, Zhang R, et al. Gelation property of alcohol-extracted soy protein isolate and effects of various reagents on the firmness of heat-induced gels. *Int J Food Prop*. (2015) 18:627–37. doi: 10.1080/10942912.2013.850508

12. Yuan E, Liu B, Ning Z. Preparation and antioxidant activity of camellianin A from *Adinandra nitida* leaves. *J Food Process Preserv*. (2008) 32:785–97. doi: 10.1111/j.1745-4549.2008.00214.x

13. Liu B, Ma Y, Liu Y, Yang Z, Zhang L. Ultrasonic-assisted extraction and antioxidant activity of flavonoids from *Adinandra nitida* leaves. *Trop J Pharm Res*. (2014) 12:1045–51. doi: 10.4314/tjpr.v12i6.27

14. Gao H, Liu B, Liu F, Chen Y. Anti-proliferative effect of camellianin A in *Adinandra nitida* leaves and its apoptotic induction in human hep G2 and MCF-7 cells. *Molecules*. (2010) 15:3878–86. doi: 10.3390/molecules15063878

15. Jia J, Bai L, Chen Y, Liu B. Inhibitory mechanism of camellianin A against α-glucosidase: in vitro and molecular simulation studies. *Foods*. (2024) 13:2835. doi: 10.3390/foods13172835

16. Zhou Y, Bai L, Geng S, Liu B. Interaction of camellianin A and lysozyme: binding mechanism and its application in nanoemulsions. *Food Chem*. (2025) 475:143265. doi: 10.1016/j.foodchem.2025.143265

17. Yang C, Liu J, Han Y, Wang B, Liu Z, Hu H, et al. Fabrication of polyphenol-pumpkin seed protein isolate (PSPI) covalent conjugate microparticles to protect free radical scavenging activity of polyphenol. *Food Biosci*. (2023) 55:102982. doi: 10.1016/j.fbio.2023.102982

18. Wang Y, Zhang P, Lin H, Fei X, Zhang G, Hu X. Covalent binding of β-Lactoglobulin and rosmarinic acid by alkaline and free-radical treatment: improved thermal stability and antioxidant capability. *Food Biosci*. (2024) 61:104574. doi: 10.1016/j.fbio.2024.104574

19. Cheng J, Dudu OE, Zhang J, Wang Y, Meng L, Wei W, et al. Impact of binding interaction modes between whey protein concentrate and quercetin on protein structural and functional characteristics. *Food Hydrocoll*. (2023) 142:108787. doi: 10.1016/j.foodhyd.2023.108787

20. Gu M, Shi J, Zhang B, Wang X, Wang X, Tian B. Interaction of soy protein isolate with hydroxytyrosol based on an alkaline method: implications for structural and functional properties. *Food Chem*. (2024) 446:138813. doi: 10.1016/j.foodchem.2024.138813

21. Du Y, Han J, Yin Z, Yan J, Jiang X, Wu H. Conjugation of (−)-epigallocatechin-3-gallate and protein isolates from large yellow croaker (*Pseudosciaena crocea*) roe: improvement of antioxidant activity and structural characteristics. *J Sci Food Agric*. (2021) 101:5948–55. doi: 10.1002/jsfa.11247

22. Ghosh V, Mukherjee A, Chandrasekaran N. Ultrasonic emulsification of food-grade nanoemulsion formulation and evaluation of its bactericidal activity. *Ultrason Sonochem*. (2013) 20:338–44. doi: 10.1016/j.ultsonch.2012.08.010

23. Li J, Gou R, Hu H, Wu X, Ai L, Wu Y. Preparation optimisation and storage stability of nanoemulsion-based lutein delivery systems. *J Microencapsul*. (2018) 35:570–83. doi: 10.1080/02652048.2018.1559245

24. Li J, Geng S, Zhen S, Lv X, Liu B. Fabrication and characterization of oil-in-water emulsions stabilized by whey protein isolate/phloridzin/sodium alginate ternary complex. *Food Hydrocoll*. (2022) 129:107625. doi: 10.1016/j.foodhyd.2022.107625

25. Ye J, Deng L, Wang Y, McClements D, Luo S, Liu C. Impact of rutin on the foaming properties of soybean protein: formation and characterization of flavonoid-protein complexes. *Food Chem*. (2021) 362:130238. doi: 10.1016/j.foodchem.2021.130238

26. Zhang Y, Lv Y, Chen L, Wu H, Zhang Y, Suo Z, et al. Inhibition of epigallocatechin-3-gallate/protein interaction by methyl-β-cyclodextrin in myofibrillar protein emulsion gels under oxidative stress. *J Agric Food Chem*. (2018) 66:8094–103. doi: 10.1021/acs.jafc.8b00275

27. Wei Y, Sun L, Gu Y, Zhuang Y, Zhang G, Fan X, et al. Rapid covalent bonding of walnut protein isolates to EGCG: unveiling the ultrasound-assisted ratio optimization, binding mechanism, and structural–functional transformations. *Foods*. (2025) 14:1204. doi: 10.3390/foods14071204

28. Tang S, Li J, Huang G, Yan L. Predicting protein surface property with its surface hydrophobicity. *Protein Pept Lett*. (2021) 28:938–44. doi: 10.2174/0929866526866210222160060

29. Moro A, Gatti C, Delorenzi N. Hydrophobicity of whey protein concentrates measured by fluorescence quenching and its relation with surface functional properties. *J Agric Food Chem*. (2001) 49:4784–9. doi: 10.1021/jf001132e

30. Shu W, Shi W, Xie H, Wang S, Zhang Q, Ouyang KF, et al. Non-covalent interaction of rice protein and polyphenols: the effects on their emulsions. *Food Chem*. (2025) 479:143732. doi: 10.1016/j.foodchem.2025.143732

31. Lang Y, Gao N, Zang Z, Meng X, Lin Y, Yang S, et al. Classification and antioxidant assays of polyphenols: a review. *J Future Foods*. (2024) 4:193–204. doi: 10.1016/j.jfutfo.2023.07.002

32. Sarikurkcu C, Ozer MS, Cakir A, Eskici M, Mete E. GC/MS evaluation and in vitro antioxidant activity of essential oil and solvent extracts of an endemic plant used as folk remedy in Turkey: *Phlomis bourgaei* Boiss. *Evid Based Complement Alternat Med*. (2013) 2013:293080. doi: 10.1155/2013/293080

33. Yi J, Fan Y, Zhang Y, Zhao L. Characterization of catechin-α-lactalbumin conjugates and the improvement in β-carotene retention in an oil-in-water nanoemulsion. *Food Chem*. (2016) 205:73–80. doi: 10.1016/j.foodchem.2016.03.005

34. Jiang P, Xiang D, Wang X. Effect of different treatment on the properties of coconut milk emulsions. *Food Sci Technol Res*. (2016) 22:83–9. doi: 10.3136/fstr.22.83

35. McClements DJ, Xiao H. Potential biological fate of ingested nanoemulsions: influence of particle characteristics. *Food Funct*. (2012) 3:202–20. doi: 10.1039/c1fo10193e

36. Song G, Li F, Xu Z, Jiang N, Wang D, Yuan T, et al. Exploring the noncovalent interaction between β-lactoglobulin and flavonoids under nonthermal process: characterization, physicochemical properties, and potential for lycopene delivering. *Food Chem X*. (2025) 25:102160. doi: 10.1016/j.fochx.2025.102160

37. Santos MAS, Okuro PK, Tavares GM, Cunha RL. Designing covalent sodium caseinate-quercetin complexes to improve emulsifying properties and oxidative stability. *Food Res Int*. (2022) 160:111738. doi: 10.1016/j.foodres.2022.111738